Supporting information for

Rational design of anti-freezing electrolyte concentrations via freeze concentration process

Liwei Jiang[1], Yuan-Chao Hu[2], Fei Ai[1], Zhuojian Liang[1], Yi-Chun Lu[1*]

1 Electrochemical Energy and Interfaces Laboratory, Department of Mechanical and Automation Engineering, The Chinese University of Hong Kong, Hong Kong SAR, China

2 Songshan Lake Materials Laboratory, Dongguan 523808, China

*Address correspondence to yichunlu@mae.cuhk.edu.hk

This file includes:
Experimental and Computational Methods
Figs. S1 to S13
Tables S1 to S14
References 1-23

Methods

Material fabrication. The $LiMn_2O_4$ cathode and PTCDI anode are purchased from MTI and Alfa Aesar corporations, respectively. The NaCoHCF cathode was prepared by a simple precipitation approach according to the literature[1]. The cathode (anode) composite electrodes were fabricated by compressing cathode (anode), carbon black, and polytetrafluorothylene (PTFE) at weight ratio of 7:2:1 (6:3:1). The Ti mesh is used as the eletrolde current collector. The 3.85 m $NaClO_4$ + 5.92 m $NaCF_3COO$ electrolyte is obtained by dissolving 3.85 mmol $NaClO_4$ and 5.92 mmol $NaCF_3COO$ into 1 g H_2O. The $H_{36}EG_{64}$-0.5 m $NaClO_4$ electrolyte is obtained by dissolving 0.5 mmol $NaClO_4$ into 0.36 g H_2O and 0.64 g ethylene glycol (EG).

Syringe-filtration method in FCE approach. In the syringe-filtration method, the dilute solution of single-solute (such as the H_2O-LiCl or H_2O-$NaClO_4$) system is usually kept in the chamber at T_t for several hours or longer time before the FCE is filtered (**Fig. S2a, ESI†**). For the multiple-solute H_2O-$NaClO_4$-$NaCF_3COO$ and $LiPFF_6$-EC-DEC system, the dilute solution is first frozen in liquid nitrogen (**Fig. S2b, ESI†**) to eliminate the supercooling during hydrate precipitation, followed by the same procedure as in above single-solute system. The equilibrium of FCEs in H_2O-LiCl, H_2O-$NaClO_4$, H_2O-$NaClO_4$-$NaCF_3COO$, and $LiPF_6$-EC-DEC systems can be reached after keeping dilute solution at T_t for 2 hours, 3 hours, 6 hours, and 24 hours, respectively, because the refractive index of obtained FCE does not change even after keeping the dilute solution at T_t for longer time. Here, the dilute solution is the one that has a concentration less than eutectic-point concentration X_e and will precipitate ice or hydrate at T_t. In the single-solute system, the electrolyte refractive index usually increases as the concentration increases. Therefore, one can identify the preselected solution as a dilute solution when the refractive index of FCE obtained at T_t is higher than that of preselected solution. The FCE concentrations in H_2O-LiCl and H_2O-$NaClO_4$ systems were determined by the refractive index method[2] (**Figs. S2c-d, ESI†**). The FCE concentrations in H_2O-$NaClO_4$-$NaCF_3COO$ system were determined by the inductively coupled plasma atomic emission spectrometry[3] (to determine the concentration of Na^+) and ion chromatography (to determine the concentration of ClO_4^-)[4, 5]. The FCE concentration in $LiPF_6$-EC-DEC system was determined by ICP test (for Li^+) and organic elemental analyzer vario EL cube (for carbon mass ratio).

Electrochemical measurements. The three-electrode cell consists of cathode (anode) composite working electrode, active carbon counter electrode, and Ag/AgCl-7.18 m LiCl (0.205 V vs. standard hydrogen electrode), with the mass ratio of counter electrode to working electrode being around 8-10. Swagelok-type cells were used to assemble the Li-based full cell, with Ti foil used to protect against halogen corrosion. Coin cells were used to assemble the Na-based full cell. The mass loadings of cathode and anode in Li-based Swagelok-type cells are 6.3 mg cm^{-2} and 7.2 mg cm^{-2} respectively. The mass loadings of cathode and anode in Na-based coin cells are 5.4 mg cm^{-2} and 7.6 mg cm^{-2} respectively. The amount of electrolyte in Li-based Swagelok-type cell and Na-based coin cell was 0.2 mL. The mass loading of cathode and anode in Li-based pouch cell are 13.3 mg cm^{-2} and 15.2 mg cm^{-2} respectively. The mass loading of cathode and anode in Na-based pouch cell are 11.4 mg cm^{-2} and 14.6 mg cm^{-2} respectively. The amount of electrolyte in Li-based and Na-based pouch cells were 1.0 mL. The charge-discharge tests of cells were performed on the Landt battery test systems (CT3001A, Wuhan Land Electronic Co., Ltd.) and Neware battery test systems (CT-4008-5V50mA-164, Neware technology limited). The full cell specific capacities are showed based on cathode mass and all the current rates are calculated based on a theoretical capacity of 120 mAh g^{-1} in both Li- and Na-based cells. The mass ratio of cathode/anode is 1/0.9 for both Li-based and Na-based full cells. The energy densities of full cells are calculated based on total active material mass of cathode and anode. For low-temperature tests, the cell performance was measured in a ShangHai BoYi B-T-107D oven.

Characterization. The refractive index was measured by the Abbe refractometer (WAY-2WAJ) with high accuracy (±0.0002). The ionic conductivities of the electrolytes were measured by electrochemical impedance spectroscopy (EIS) using BioLogic. The chemical formula ($Na_{1.4}Co[Fe(CN)_6]_{0.84}\cdot 2.5H_2O$) of NaCoHCF cathode was determined by inductively coupled plasma atomic emission spectrometry. The Raman spectra for electrolytes were conducted on HORIBA HR evolution microscope using a 532 nm excitation laser. The Raman spectra of H_2O-$NaClO_4$ system at –34.1 ^oC and H_2O-$NaClO_4$-$NaCF_3COO$ system at –50 ^oC were tested after experiencing a cooling process from 25 ^oC to –150 ^oC. DSC tests were carried out in DSC200F3 with cooling and heating rates of 10 K min^{-1} from 25 ^oC to –150 ^oC. The linear sweep voltammetry (LSV) is tested at scan rate of 10 mV s^{-1} using BioLogic.

AIMD simulations. The AIMD simulations were carried out by using the Vienna ab initio simulation package (VASP)[6]. The projector augmented-wave (PAW) potentials[7] generated with Perdew–Burke–Ernzerhof (PBE) generalized gradient approximation (GGA)[8]were used. The van der Waals (vdW) interaction was taken into account by using the rev-vdWDF2 functional[9]. The plane wave cut-off energy was set to 400 eV and the Γ point was used for the Brillouin zone sampling. The AIMD simulations were performed in a canonical ensemble (NVT)[10, 11] by using a Nose-Hoover thermostat at 300 K (H_2O, 7.18 m LiCl, 9.07 m $NaClO_4$, 3.85 m $NaClO_4$ + 5.92 m $NaCF_3COO$), with a time step of 1 fs. All the AIMD simulations were run for 60-100 ps to yield the data for analysis. The H_2O AIMD model contains 165 atoms (55 H_2O) within 11.8 Å x 11.8 Å x 11.8 Å cubic supercell. The 7.18 m LiC electrolyte AIMD model contains 181 atoms (8 LiCl and 55 H_2O) within 12.5 Å x 12.5 Å x 12.5 Å cubic supercell. The 9.07 m $NaClO_4$ electrolyte AIMD model contains 96 atoms (4 $NaClO_4$ and 24 H_2O) within 10.5 Å x 10.5 Å x 10.5 Å cubic supercell. The 3.85 m $NaClO_4$ + 5.92 m $NaCF_3COO$ electrolyte AIMD model contains 117 atoms (2 $NaClO_4$, 3 $NaCF_3COO$, and 27 H_2O) within 11.5 Å x 11.5 Å x 11.5 Å cubic supercell. The initial structures of liquid electrolyte models were constructed using the Packmol software[12].

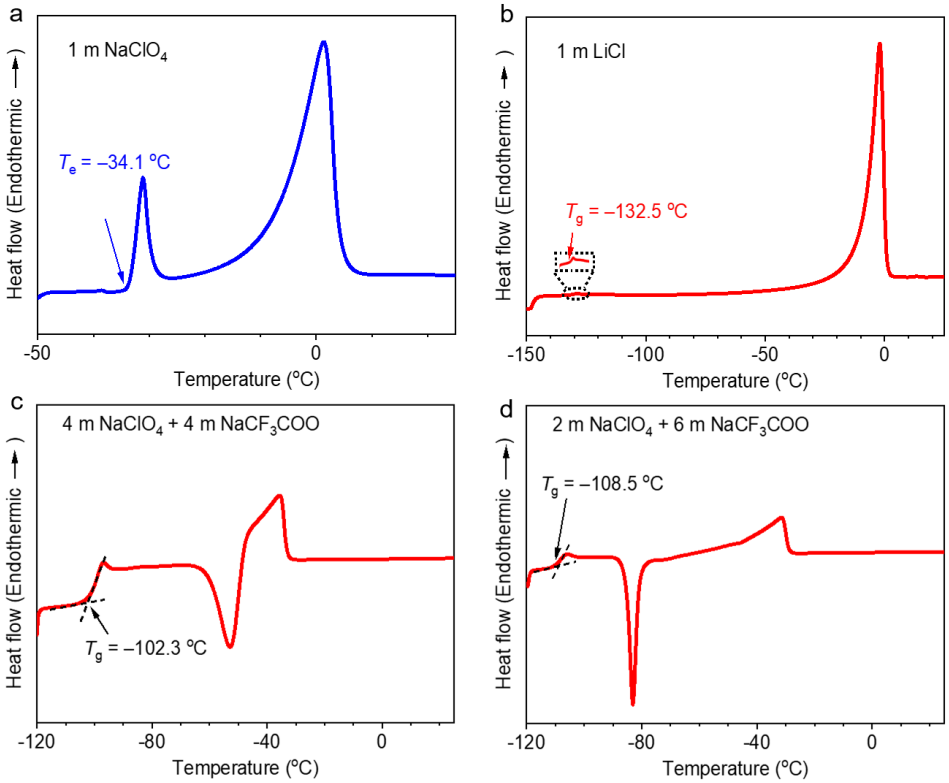

Fig. S1. Determine the liquid-to-solid low-temperature limits of H_2O-solute systems by DSC heating curves of dilute solutions. (a) The DSC heating curve of 1 m $NaClO_4$ electrolyte in H_2O-$NaClO_4$ system. The eutectic heat-flow peak on the DSC curve demonstrates that the thermodynamic liquid-to-solid low-temperature limit T_e of the H_2O-$NaClO_4$ system is –34.1 °C. T_e is usually determined by the onset temperature of T_e peak[13]. **(b)** The DSC heating curve of 1 m LiCl electrolyte in H_2O-LiCl system. The DSC curve shows the glass-transition step (see the enlarged picture in the dotted rectangle) rather than the eutectic heat-flow peak, demonstrating that the DSC test can only determine the kinetic liquid-to-solid low-temperature limit T_g (–132.5 °C) rather than the T_e value of H_2O-LiCl system. T_g is usually determined by the onset temperature of T_g peak[14]. **(c-d)** The DSC heating curves of 4 m $NaClO_4$ + 4 m $NaCF_3COO$ (T_g = –102.3 °C) **(c)** and 2 m $NaClO_4$ + 6 m $NaCF_3COO$ (T_g = –108.5 °C) **(d)** electrolytes in H_2O-$NaClO_4$-$NaCF_3COO$ system.

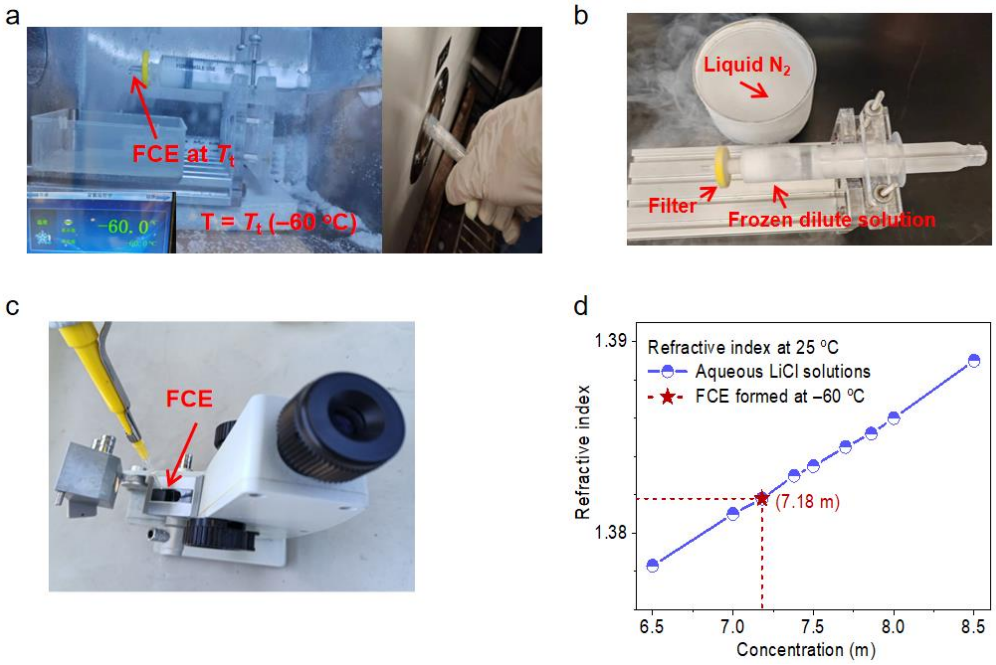

Fig. S2. The syringe-filtration method for the FCE approach. (a) keep the dilute solution in the chamber at T_t (e.g. –60 °C) to reach chemical equilibrium before filtering the FCE by manually squeezing the syringe. **(b)** Illustration of a dilute solution of H_2O-$NaClO_4$-$NaCF_3COO$ system being frozen in liquid N_2. **(c)** Measure the refractive index of FCE with the Abbe refractometer. **(d)** Determine the concentration of FCE obtained at –60 °C by the refractive index method.

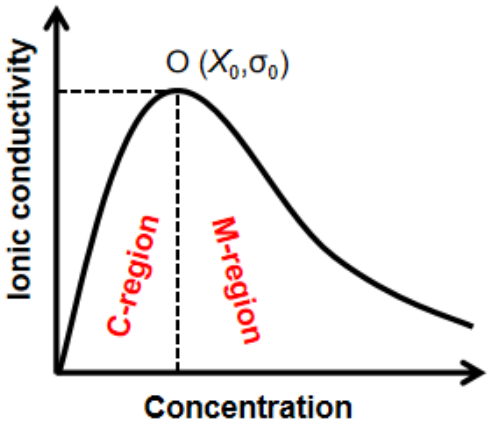

Fig. S3. Typical concentration-conductivity curve in an H_2O-solute system. The point O (X_0, σ_0) is the maximum conductivity point. The concentration-conductivity curve can be divided into two regions[15, 16]: concentration-controlled region (C-region) below concentration X_0 and mobility-controlled region (M-region) above concentration X_0. The FCE obtained at ultralow T_t usually locate at the M-region and therefore has the lowest electrolyte concentration (therefore the lowest cost) and the highest ionic conductivity without being frozen at T_t.

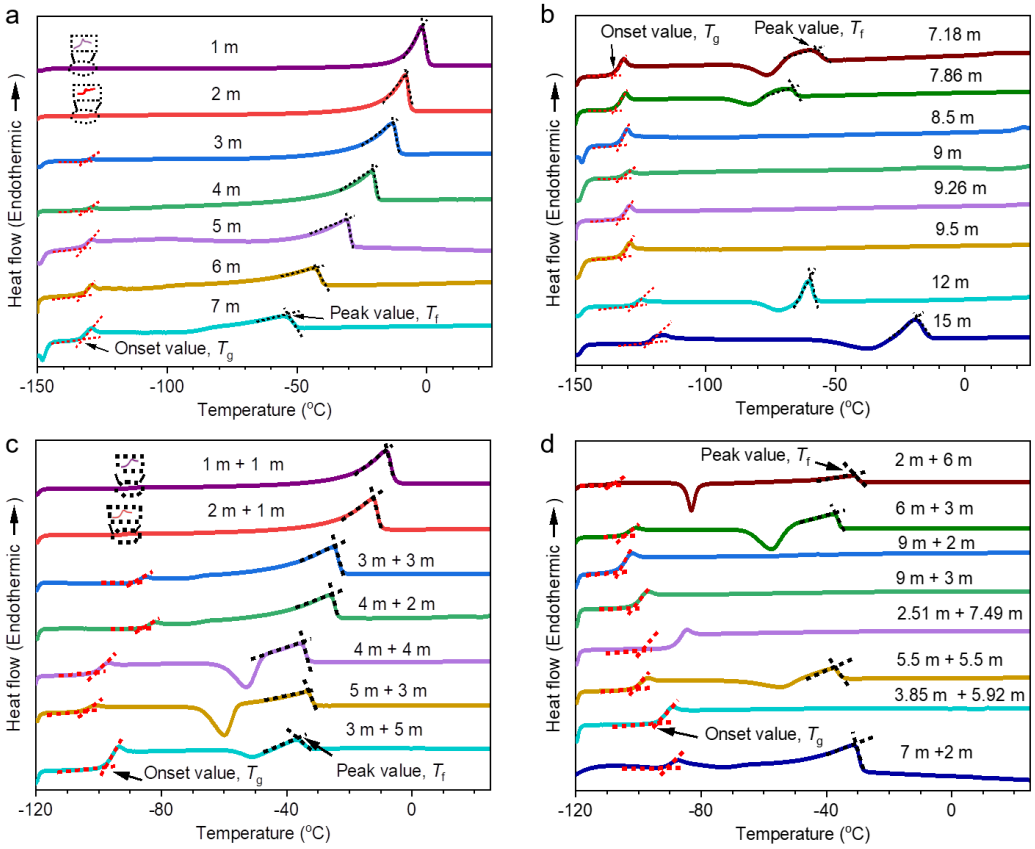

Fig. S4. The DSC heating curves of aqueous solutions in H_2O-LiCl and H_2O-$NaClO_4$-$NaCF_3COO$ systems at heating rate of 10 K min^{-1}. a-b, 1 m to 15 m LiCl**. c-d, Various electrolyte concentrations.** The "1 m + 1 m" represents the "1 m $NaClO_4$ + 1 m $NaCF_3COO$". See all the T_g and T_f values in **Tables S2 and S8**.

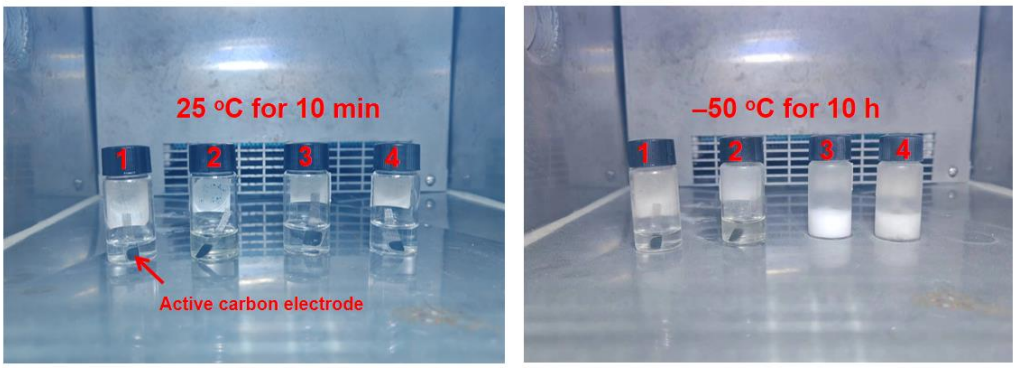

Fig. S5. The photographs of various electrolytes in H_2O-$NaClO_4$-$NaCF_3COO$ system at 25 °C (10 min) and –50 °C (10 h). The active carbon electrodes are used to inhibit supercooling phenomenon and promote electrolyte crystallization. No. 1: 3.85 m $NaClO_4$ + 5.92 m $NaCF_3COO$, No. 2: 7.49 m $NaClO_4$ +2.51 m $NaCF_3COO$, No. 3: 9 m $NaClO_4$ + 2 m $NaCF_3COO$, No. 4: 9 m $NaClO_4$ + 3 m $NaCF_3COO$.

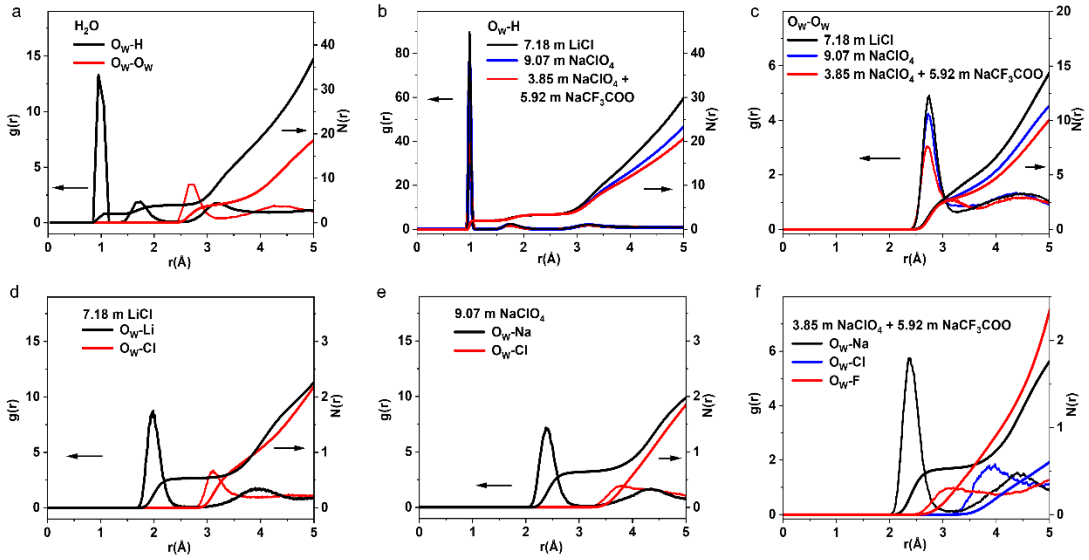

Fig. S6. The radial distribution function g(r) and coordination number N(r) for pure H_2O, 7.18 m LiCl, 9.07 m $NaClO_4$, 3.85 m $NaClO_4$ + 5.92 m $NaCF_3COO$ AIMD models. (a) Ow-H and Ow-Ow in pure H_2O. (**b**) Ow-H in the designed FCEs. (**c**) Ow-Ow in the designed FCEs. **(d)** Ow-Li and Ow-Cl in 7.18 m LiCl. **(e)** Ow-Na and Ow-Cl in 9.07 m $NaClO_4$. **(f)** Ow-Na, Ow-Cl, and Ow-F in 3.85 m $NaClO_4$ + 5.92 m $NaCF_3COO$**.** Ow: oxygen atom in H_2O.

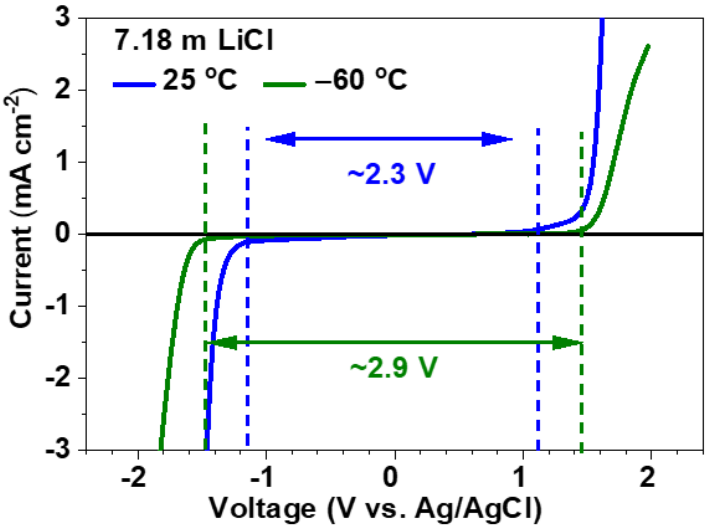

Fig. S7. The linear sweep voltammetry (Scan rate: 10 mV s^{-1}) of 7.18 m LiCl electrolyte at 25 °C and –60 °C.

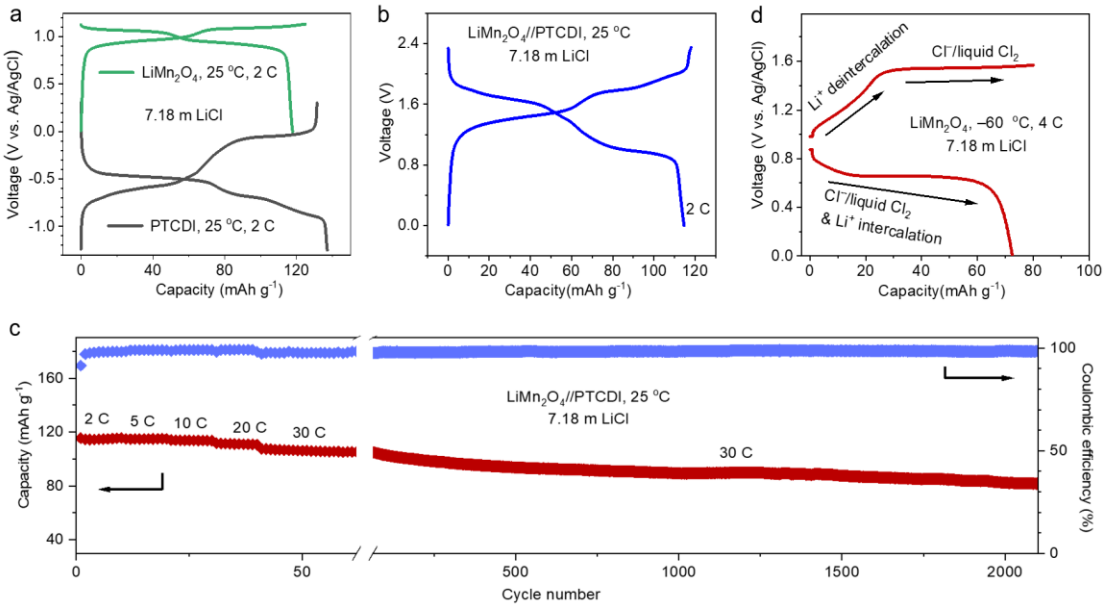

Fig. S8. Performances of Li-based electrodes and cells in 7.18 m LiCl electrolyte. (a-b), Typical charge-discharge curves of $LiMn_2O_4$ cathode (**a**), PTCDI anode (**a**), and $LiMn_2O_4$//PTCDI full cell (**b**) at 25 °C. **(c)** Rate capability and cycling stability of $LiMn_2O_4$//PTCDI full cell at 25 °C. **(d)** Typical charge-discharge curve of $LiMn_2O_4$ cathode at –60 °C. The reversible capacity at –60 °C is contributed by Li^+-(de)intercalation mechanism and Cl^-/liquid Cl_2 redox mechanism.

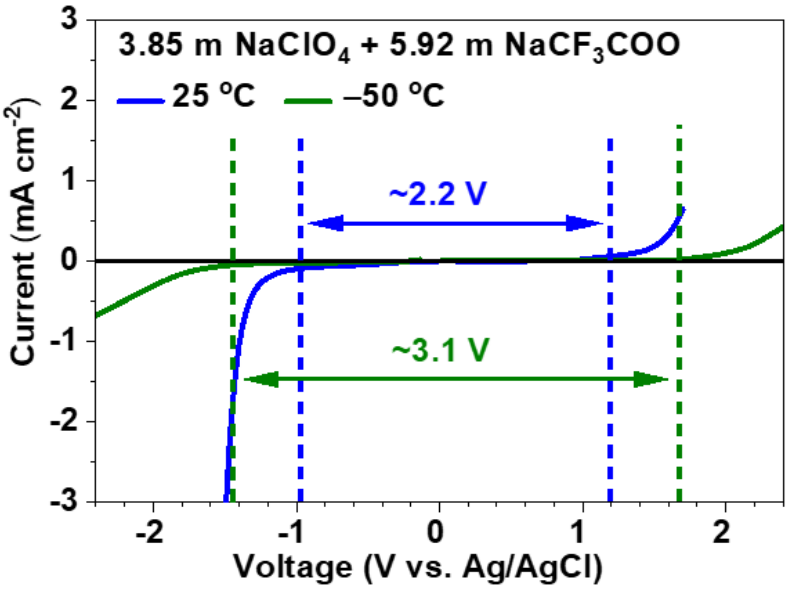

Fig. S9. The linear sweep voltammetry (Scan rate: 10 mV s^{-1}) of 3.85 m $NaClO_4$ + 5.92 m $NaCF_3COO$ electrolyte at 25 °C and –50 °C.

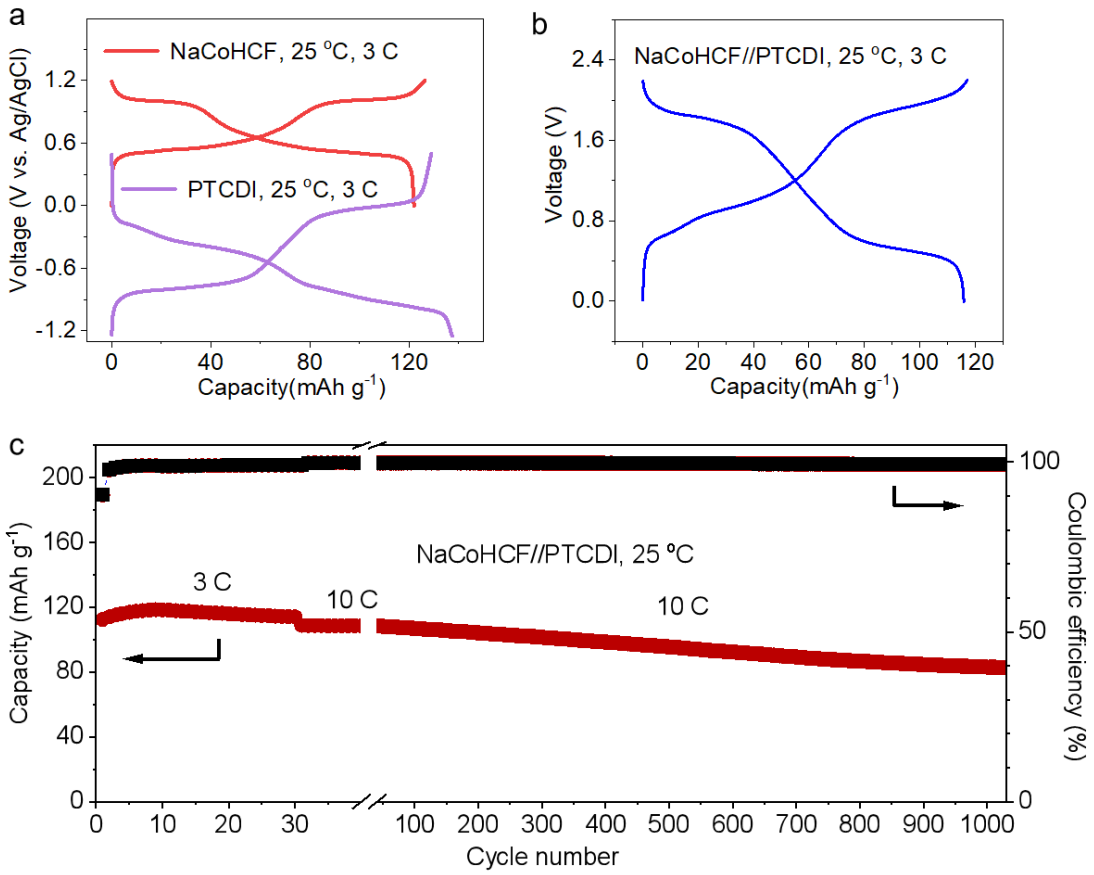

Fig. S10. Performances of Na-based electrodes and cells in 3.85 m $NaClO_4$ + 5.92 m $NaCF_3COO$ electrolyte. (a-b) Typical charge-discharge curves of NaCoHCF cathode (**a**), PTCDI anode (**a**), and NaCoHCF//PTCDI full cell (**b**) at 25 ºC. **(c)** Rate capability and cycling stability of NaCoHCF//PTCDI full cell at 25 ºC.

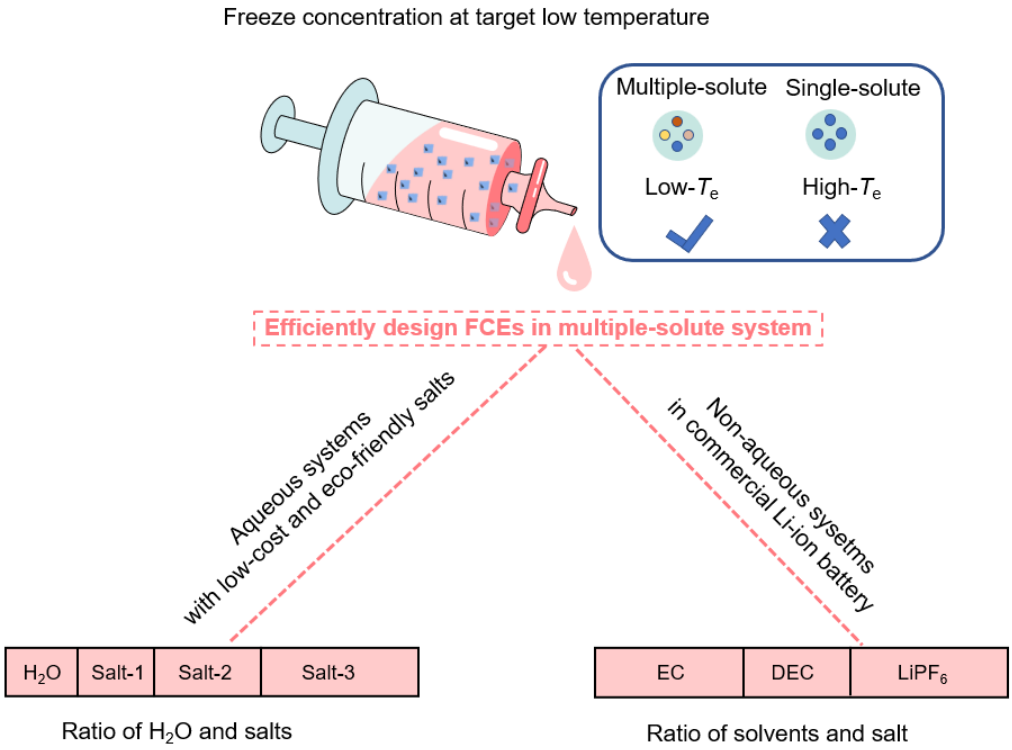

Fig. S11. Future applications of the FCE approach in designing anti-freezing electrolytes. EC: ethylene carbonate. DEC: dimethyl carbonate.

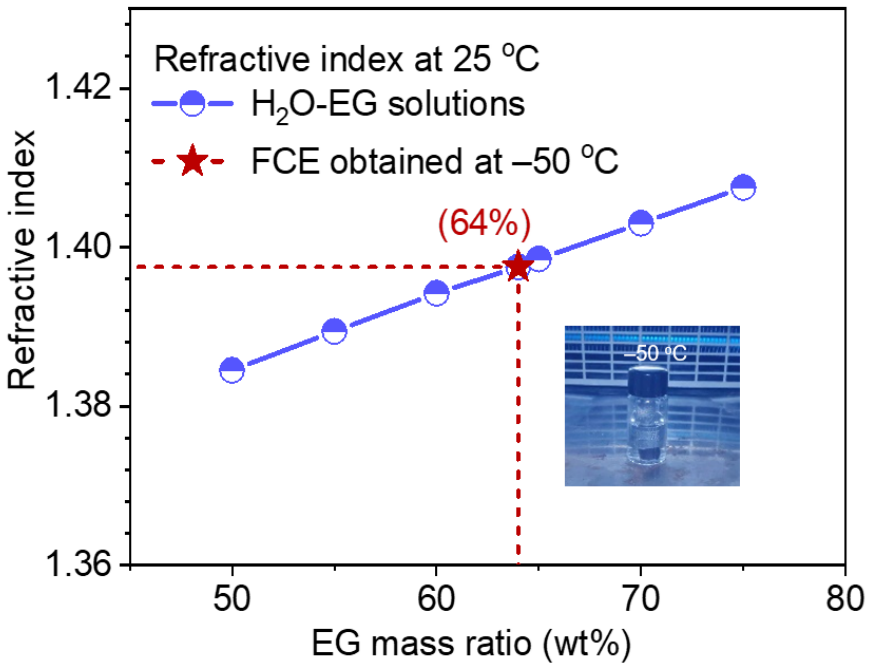

Fig. S12. Design anti-freezing electrolyte in H_2O-EG-$NaClO_4$ system using FCE approach when T_t is –50 °C. Here, we firstly determined the lowest EG amount (64 wt%) needed to keep unfrozen state in H_2O-EG system, and then prepared the $H_{36}EG_{64}$-0.5 m $NaClO_4$ electrolyte. The electrolyte can maintain unfrozen state at –50 °C, as shown in the inset photograph (The active carbon electrode is used to inhibit supercooling phenomenon and promote electrolyte crystallization).

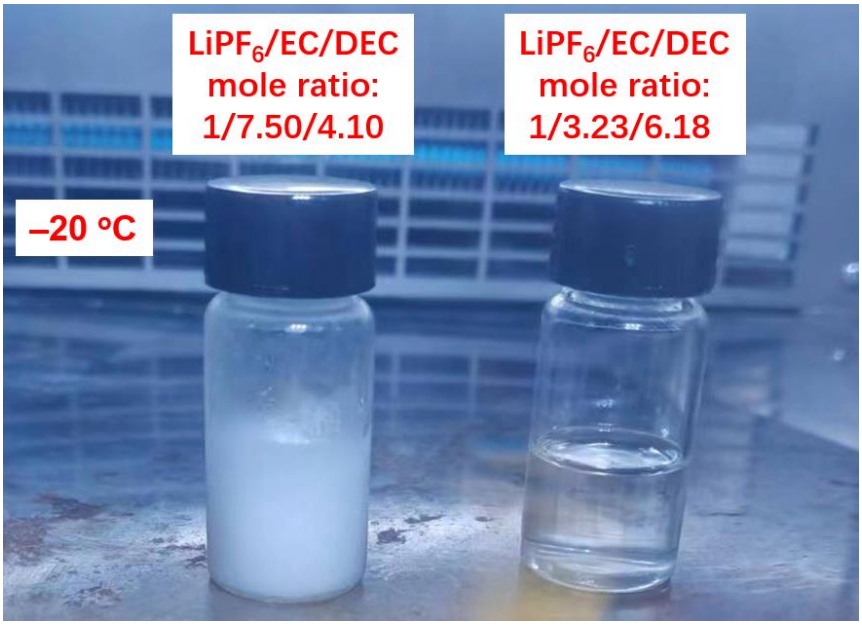

Fig. S13. The picture of dilute solution (left) and determined FCE (right) after keeping at –20 °C for 24 h (firstly being frozen in liquid N_2). The dilute solution is the typical commercial formula, 1M $LiPF_6$ in EC-DEC (1:1, vol) (mole ratio of $LiPF_6$/EC/DEC is 1/7.50/4.10). The FCE component mole ratio $LiPF_6$/EC/DEC is determined as 1/3.23/6.18 (**Table S14, ESI†**).

Table S1. The definition of the symbols in the main text.

Symbols	Definition
T_f	Freezing point
T_e	Eutectic temperature
T_t	The target low temperature
T_g	Glass-transition temperature
T_D	Freezing point of dilute solution
X_e	Eutectic-point concentration
X_D	Concentration of dilute solution
X_F	Concentration of FCE
$X_{salt\text{-}1}$, $X_{salt\text{-}2}$, and X_{H_2O}	Concentration percentages of FCE concentration in ternary systems

Table S2. The T_g and T_f values of aqueous solutions in H_2O-LiCl system based on the DSC data in Figs. S4a-b and the design efficiency in conventional approach. The "*" means that the T_f values of these electrolytes cannot be determined by DSC curves owing to the lack of melting peaks, but their T_f are lower than –60 ºC according to the reported H_2O-LiCl phase diagram[17].

Preselected concentration	T_g determined by DSC	T_f determined by DSC	Preselected numbers	Qualifying numbers	Design efficiency
1 m	–132.5 ºC	–1.5 ºC	15	5	33.3%
2 m	–132.5 ºC	–8.1 ºC			
3 m	–132.5 ºC	–12.8 ºC			
4 m	–132.5 ºC	–20.4 ºC			
5 m	–132.6 ºC	–30.5 ºC			
6 m	–132.4 ºC	–42.5 ºC			
7 m	–132.5 ºC	–53.3 ºC			
7.18 m	–135.3 ºC	–56.8 ºC			
7.86 m	–134.5 ºC	–66.5 ºC			
8.5 m*	–133.4 ºC	\			
9 m*	–132.9 ºC	\			
9.26 m*	–132.5 ºC	\			
9.5 m*	–132.1 ºC	\			
12 m	–128.5 ºC	–58.9 ºC			
15 m	–121.3 ºC	–18.9 ºC			

Table S3. The anti-freezing electrolyte design using FCE approach when T_t is set as –60 °C in H_2O-LiCl system and the design efficiency in FCE approach.

Preselected concentration	Refractive index of FCE at 25 °C	FCE concentration	Qualifying / Preselected numbers	Design efficiency
3 m	1.3818	7.18 m	4/4	100%
4 m	1.3818	7.18 m		
5 m	1.3818	7.18 m		
6 m	1.3818	7.18 m		

Table S4. The ionic conductivities of various aqueous LiCl electrolytes at –60 °C.

Concentration	Ionic conductivity at –60 °C (mS cm^{-1})
5 m	3.44
6 m	4.27
6.75 m	5.08
7.18 m	6.09
7.86 m	5.87
8.5 m	5.56
9.26 m	5.12
10 m	4.81

Table S5. The eutectic-point concentration X_e of H_2O-$NaClO_4$ system identified via FCE approach (T_t = –34.1 °C).

Preselected concentration	Refractive index of FCE at 25 °C	X_e
4 m	1.3745	9.07 m
5 m	1.3745	9.07 m
6 m	1.3745	9.07 m

Table S6. The eutectic-point concentration X_e for various H_2O-solute system determined by FCE approach. All the T_e values of H_2O-solute systems are determined by DSC tests.

System	Targeted temperature (T_e)	Refractive index of FCE at 25 °C	X_e
H_2O-$NaCF_3SO_3$	–20.5 °C	1.3470	4.54 m
H_2O-KCF_3SO_3	–20.5 °C	1.3530	8.30 m
H_2O-$LiBF_4$	–28.5 °C	1.3206	4.53 m
H_2O-KCl	–12.2 °C	1.3610	3.42 m
H_2O-LiTFSI	–42.5 °C	1.3584	5.41 m
H_2O-NaCl	–21.1 °C	1.3705	5.11 m

Table S7. The anti-freezing electrolyte design using FCE approach when T_t is set as –50 °C in H_2O-$NaClO_4$-$NaCF_3COO$ system and the design efficiency in FCE approach.

Preselected concentration ($NaClO_4$ + $NaCF_3COO$)	Refractive index of FCE at 25 °C	FCE concentration	Qualifying / Preselected numbers	Design efficiency
4 m + 4 m	1.3615	3.85 m + 5.92 m	2/2	100%
2 m + 6 m	1.3593	2. 51m + 7.49 m		

Table S8. The T_g and T_f values of aqueous solutions in H_2O-$NaClO_4$-$NaCF_3COO$ system based on the DSC data in Figs. S4c-d and the design efficiency in conventional approach. The "*" means that the T_f values of these electrolytes cannot be determined by DSC curves owing to the lack of melting peaks. According to our crystallization acceleration test in **Fig. S5**, the two electrolytes (9 m + 2 m, 9 m + 3 m) freeze at –50 ºC, whereas another two electrolytes (3.85 m + 5.92 m, 2.51 m + 7.49 m) do not freeze at –50 ºC.

Preselected concentration $NaClO_4$ + $NaCF_3COO$	**T_g determined by DSC**	**T_f determined by DSC**	**Qualifying /Preselected numbers**	**Design efficiency**
1 m + 1 m	–91.4 ºC	–8.1 ºC	2/15	13.3%
2 m + 1 m	–93.6 ºC	–12.3 ºC		
3 m + 3 m	–88.6 ºC	–24.3 ºC		
4 m + 2 m	–85.3 ºC	–25.6 ºC		
4 m + 4 m	–100.6 ºC	–34.7 ºC		
5 m + 3 m	–104.1 ºC	–32.9 ºC		
3 m + 5 m	–97.5 ºC	–36.2 ºC		
2 m + 6 m	–108.5 ºC	–30.8 ºC		
6 m + 3 m	–104.4 ºC	–37.1 ºC		
9 m + 2 m*	–106.2 ºC	\		
9 m + 3 m*	–101.5 ºC	\		
7 m + 2 m*	–99.1 ºC	–30.8 ºC		
5.5 m + 5.5 m	–101.4 ºC	–36.9 ºC		
3.85 m + 5.92 m*	–93.7 ºC	\		
2.51 m + 7.49 m*	–88.2 ºC	\		

Table S9. The ionic conductivities of FCEs (T_t = –50 °C) in H_2O-$NaClO_4$-$NaCF_3COO$ systems.

Electrolytes ($NaClO_4$ + $NaCF_3COO$)	Ionic conductivity at 25 °C (mS cm^{-1})	Ionic conductivity at –50 °C (mS cm^{-1})
3.85 m + 5.92 m	96.9	0.31
2.51 m + 7.49 m	86.7	0.24

Table S10. The coordination species and numbers within cutoff radius of 4 Å based on AIMD results.

Liquid structures	Coordination species and numbers (cutoff radius: 4 Å)					
	O_W-H	**O_W-O_W**	**O_W-Li**	**O_W-Cl**	**O_W-Na**	**O_W-F**
H_2O	19.7	7.4	\	\	\	\
7.18 m LiCl	15.9	6.6	1.16	1.07	\	\
9.07 m $NaClO_4$	13.1	5.3	\	0.88	0.58	\
3.85 m $NaClO_4$ + 5.92 m $NaCF_3COO$	12.0	4.7	\	0.19	0.73	0.91

Table S11. Compared Li-based FCE to reported electrolytes in terms of ionic conductivity, battery operating low-temperature limit (OLTL), energy density at 25 °C, and lifespan.

Systems	Electrolyte	Ionic Conductivity	OLTL, Energy density, lifespan
$LiMn_2O_4$//PTCDI **(This work)**	7.18 m LiCl	6.09 mS cm^{-1}, –60 °C	–60 °C, 80 Wh kg^{-1}, >2000 cycles
$LiMn_2O_4$//Mo_6S_8 (Literature)[18]	5 m LiTFSI-CO_2	~1.5 mS cm^{-1}, –40 °C	–40 °C, ~80 Wh kg^{-1}, 2000 cycles
$LiMn_2O_4$//CuSe (Literature)[19]	7.86 m LiCl	5.00 mS cm^{-1}, –78 °C,	–78 °C, 109 Wh kg^{-1}, 100 cycles
$LiMn_2O_4$//$LiTi_5O_{12}$ (Literature)[20]	H_2O-DOL-LiTFSI (BSiS-$DOL_{0.5}$)	0.1 mS cm^{-1}, –50 °C,	–50 °C, /, 100 cycles

Table S12. Compared Na-based FCE to reported electrolytes in terms of other cation, co-solvent, battery operating low-temperature limit (OLTL), energy density at 25 °C, and lifespan.

Systems	Electrolyte	Other cation or Co-solvent	OLTL, Energy density, lifespan
NaCoHCF//PTCDI **(This work)**	3.85 m $NaClO_4$ + 5.92 m $NaCF_3COO$	No	–50 °C, 62 Wh kg^{-1}, >1000 cycles
$Na_3(VOPO_4)_2F$//$NaTi_2(PO_4)_3$ (Literature)[21]	25 m NaFSI + 10 m NaFTFSI	No	–10 °C, 64 Wh Kg^{-1}, 500 cycles
NaCoHCF//AC (Literature)[22]	1 m $NaClO_4$ + 3.86 m $CaCl_2$	Yes (Ca^{2+})	–30 °C, 28 Wh kg^{-1}, 1000 cycles
AC//$NaTi_2(PO_4)_3$ (Literature)[23]	$H_2O_{0.7}DMSO_{0.3}$-2 m $NaClO_4$	Yes (DMSO)	–50 °C, 36 Wh kg^{-1}, 100 cycles

Table S13. The anti-freezing electrolyte design using FCE approach when T_t is set as –50 °C in H_2O-EG-$NaClO_4$ system.

Preselected concentration (mass ratio)	FCE concentration (mass ratio)	Prepared electrolyte concentration
H_2O-EG (60:40)	H_2O-EG (36:64)	$H_{36}EG_{64}$-0.5 m $NaClO_4$

Table S14. The anti-freezing electrolyte design using FCE approach when T_t is set as –20 °C in $LiPF_6$-EC-DEC system.

Preselected concentration (mole ratio)	FCE concentration (mole ratio)
$LiPF_6$-EC-DEC (1:7.50:4.10)	$LiPF_6$-EC-DMC (1:3.23:6.18)

References:

1. X. Wu, M. Sun, S. Guo, J. Qian, Y. Liu, Y. Cao, X. Ai and H. Yang, *ChemNanoMat.*, 2015, **1**, 188-193.
2. C.-Y. Tan and Y.-X. Huang, *J. Chem. Eng. Data*, 2015, **60**, 2827-2833.
3. D. Butcher, *Instrum. Sci. Technol.*, 2010, **38**, 458-469.
4. R. Michalski, *Crit. Rev. Anal. Chem.*, 2006, **36**, 107-127.
5. A. Buzid, J. Boertjes, E. S. Gilchrist, J. D. Glennon and J. H. T. Luong, *Anal. Methods*, 2023, **15**, 3382-3392.
6. G. Kresse and J. Furthmüller, *Phys. Rev. B*, 1996, **54**, 11169.
7. G. Kresse and J. Furthmüller, *Comput. Mater. Sci.*, 1996, **6**, 15-50.
8. J. P. Perdew, K. Burke and M. Ernzerhof, *Phys. Rev. Lett.*, 1996, **77**, 3865.
9. M. Dion, H. Rydberg, E. Schroder, D. C. Langreth and B. I. Lundqvist, *Phys. Rev. Lett.*, 2004, **92**, 246401.
10. S. Nosé, *J. Chem. Phys.*, 1984, **81**, 511-519.
11. W. G. Hoover, *Phys. Rev. A*, 1985, **31**, 1695.
12. L. Martínez, R. Andrade, E. G. Birgin and J. M. Martínez, *J. Comput. Chem.*, 2009, **30**, 2157-2164.
13. M. Ding, K. Xu and T. Jow, *J. Therm. Anal. Calorim.*, 2000, **62**, 177-186.
14. Q. Wang, L. Zhao, C. Li and Z. Cao, *Sci. Rep.*, 2016, **6**, 26831.
15. L. Jiang, L. Liu, J. Yue, Q. Zhang, A. Zhou, O. Borodin, L. Suo, H. Li, L. Chen, K. Xu and Y. S. Hu, *Adv. Mater.*, 2020, **32**, 1904427.
16. V. V. Shcherbakov, *Russ. J. Electrochem.*, 2009, **45**, 1292-1295.
17. C. Monnin, M. Dubois, N. Papaiconomou and J.-P. Simonin, *J. Chem. Eng. Data*, 2002, **47**, 1331-1336.
18. J. Yue, J. Zhang, Y. Tong, M. Chen, L. Liu, L. Jiang, T. Lv, Y. S. Hu, H. Li, X. Huang, L. Gu, G. Feng, K. Xu, L. Suo and L. Chen, *Nat. Chem.*, 2021, **13**, 1061-1069.
19. L. Tang, Y. Xu, W. Zhang, Y. Sui, A. Scida, S. R. Tachibana, M. Garaga, S. K. Sandstrom, N. C. Chiu, K. C. Stylianou, S. G. Greenbaum, P. A. Greaney, C. Fang and X. Ji, *Angew. Chem. Int. Ed.*, 2023, **62**, e202307212.
20. Z. Ma, J. Chen, J. Vatamanu, O. Borodin, D. Bedrov, X. Zhou, W. Zhang, W. Li, K. Xu and L. Xing, *Energy Storage Mater.*, 2022, **45**, 903-910.
21. D. Reber, R.-S. Kühnel and C. Battaglia, *ACS Mater. Lett.*, 2019, **1**, 44-51.

22. K. Zhu, Z. Li, Z. Sun, P. Liu, T. Jin, X. Chen, H. Li, W. Lu and L. Jiao, *Small*, 2022, **18**, 2107662.
23. Q. Nian, J. Wang, S. Liu, T. Sun, S. Zheng, Y. Zhang, Z. Tao and J. Chen, *Angew. Chem. Int. Ed.*, 2019, **58**, 16994-16999.